

CHARACTERIZATION OF INTERACTIONS BETWEEN BUBBLES AND FLUID TURBULENCE UTILIZING PTV-BASED SGS

Tomohiko Tanaka

Central Research Laboratory
Hitachi, Ltd.

1–280 Higashi-Koigakubo, Kokubunji, Tokyo, 185–8601, Japan
tomohiko.tanaka.nx@hitachi.com

Yohei Sato and Koichi Hishida

Department of System Design Engineering
Keio University

3–14–1 Hiyoshi, Kohoku-ku, Yokohama, 223–8522, Japan
yohei@sd.keio.ac.jp, hishida@sd.keio.ac.jp

ABSTRACT

The mechanisms of turbulence modification by dispersed bubbles in an upward bubbly pipe flow were investigated. The liquid-phase velocity was measured by particle tracking velocimetry with Sub-Kolmogorov time and spatial resolution. Sub-Kolmogorov resolution is high enough to obtain small scale structures of the modified turbulence by bubbles. Gas-phase behaviors were measured by a shape projection imaging technique. Two different bubble diameters at the void fraction up to 1.5% were examined. The profiles of mean streamwise velocity of water were flattened in the pipe middle region, because the bubbles accumulated near the pipe wall accelerated the fluid. The flattened mean flow profiles suppressed the shear-induced turbulence intensities. In the present study, we introduced a scaling method by expanding the spatial filtering techniques applied for measured velocity fields to characterize length scales that govern the energy transfer between bubbles and turbulence. Large energy transport from bubbles to the fluids was clearly observed at the scale of from 2 to 3 times the bubble diameter. The findings above give guidance on the physics and modeling of multiphase turbulence.

INTRODUCTION

Bubbly flows are observed in many engineering applications such as chemical reactors and power plants, although details of the bubbly flows are not fully understood due to their complexity. In turbulent bubbly flow studies, there are two main research interests: turbulence modification by bubbles and bubble behaviors. Previous studies of turbulence modification have shown that dispersed bubbles can either augment or attenuate the liquid-phase turbulent kinetic energy (TKE) (Serizawa *et al.*, 1975; Theofanous & Sullivan, 1982; Wang *et al.*, 1987; Fujiwara *et al.*, 2004). Though it is also known that bubbles also modified the TKE energy spectrum (Lance & Bataille, 1991; Mudde *et al.*, 1997), their modification patterns of the spectrum were different, and it is still difficult to state clearly the well defined mechanisms of turbulence modification. This is because the underlying physical energy transport mechanisms are not well understood.

The objective of the present study is to experimentally investigate the TKE transport mechanism among bubbles, large and small eddies, which affect the overall turbulence modification, by using particle tracking velocimetry (PTV) with Sub-Kolmogorov time and spatial resolution. The premise is that a detailed understanding of the microscopic interactions between bubbles and turbulence will lead to improve understanding and prediction of the macroscopic turbulence modification. Bubble behaviors were obtained by shape projection imaging (SPI). A scaling analysis was performed to characterize length scales that govern the energy transport between bubbles and turbulence by expanding the spatial filtering techniques applied for measured velocity fields.

EXPERIMENTAL SETUP

Figure 1 shows the schematic of the experimental facility used in this study. The facility is the same as that used for the study of Fujiwara *et al.* (2004). While a thorough description is described in their article, the important aspects of the experimental facility are recounted below.

Bubbly Flow Description

Details of the fully developed upward flow used in the present study are summarized in Table 1. Optical distortion through the pipe was eliminated using a fluorinated ethylene propylene (FEP) pipe at the test section. FEP has almost the same refraction index as water. The test section was covered with a rectangular acrylic container filled with water to have straight optical access into the pipe.

Bubbles were injected by a bubble generator attached at the entrance of the pipe. The bubble parameters are listed in table 2. The void fraction was set to be 0.5 %, 1.0 % or 1.5 % by adjusting the air pressure of the bubble generator to examine the effects of void fraction on turbulence modification. Two different bubble diameters were examined by adding a surfactant of 3-pentanol ($C_5H_{11}OH$), because the presence of the surfactant avoids bubble coalescence resulting in the smaller bubbles. The mean area equivalent diameter, $\langle d_{eq} \rangle$, was estimated by the captured images.

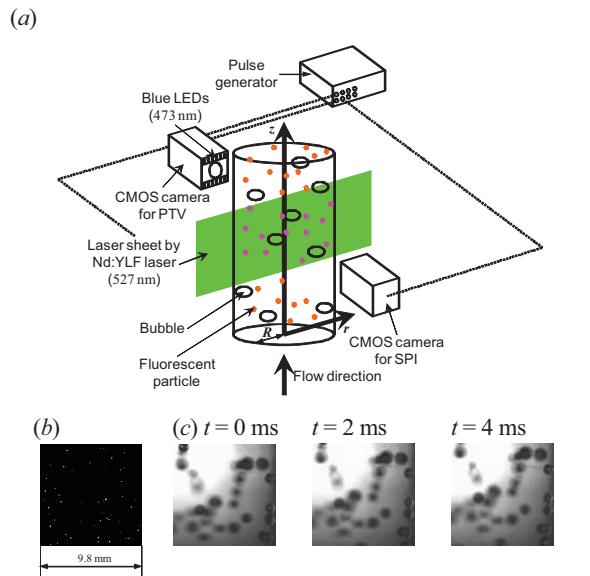


Figure 1 : (a) Schematic of experimental apparatus. (b) Instantaneous image by PTV and (c) by SPI.

| Parameter | Symbol | Unit | Value |
|------------------------------|----------------------------|----------------------|-------|
| Pipe diameter | $2R$ | (mm) | 44 |
| Centerline mean velocity | $\langle U_c \rangle$ | (mm/s) | 247 |
| Bulk mean velocity | $\langle U_{bulk} \rangle$ | (mm/s) | 200 |
| Pipe Reynolds number | Re_{2R} | | 9,900 |
| Kinematic viscosity of water | ν | (mm ² /s) | 0.81 |
| Kolmogorov length scale† | η | (μ m) | 330 |
| Kolmogorov time scale† | τ_K | (ms) | 120 |

†value at pipe centerline

| Without surfactant | | | | |
|--------------------------|------|-------|-------|-------|
| α | (%) | 0.5 | 1.0 | 1.5 |
| $\langle d_{eq} \rangle$ | (mm) | 2.39 | 2.58 | 2.62 |
| Stan. dev. | (mm) | 0.60 | 0.66 | 0.64 |
| Skewness | (-) | -0.11 | -0.11 | -0.45 |
| With surfactant | | | | |
| α | (%) | 0.5 | 1.0 | 1.5 |
| $\langle d_{eq} \rangle$ | (mm) | 1.59 | 1.71 | 1.76 |
| Stan. dev. | (mm) | 0.34 | 0.31 | 0.30 |
| Skewness | (-) | -0.04 | -0.01 | -0.03 |

Measurement System

The measurement system consists of high time/spatial resolution PTV and a bubble shape projection imaging technique as described in figure 1. Two CMOS cameras were located facing each other near the test section and synchronized by a pulse generator to simultaneously capture both liquid and gaseous phases.

For PTV, an Nd:YLF laser (Quantronix Corp., Falcon 527DP) with a wavelength of 527 nm and the energy of each pulse was 30 mJ was used as the light source. Fluorescent tracers (Lefranc et Bourgeois, S.A., Light Orange Fluo) with a fluorescence wavelength of about 600 nm were selected so that it is possible to capture only fluorescent tracer images by cutting the laser scattering at the bubble surfaces using a color filter. The PTV time resolution was the same as the camera

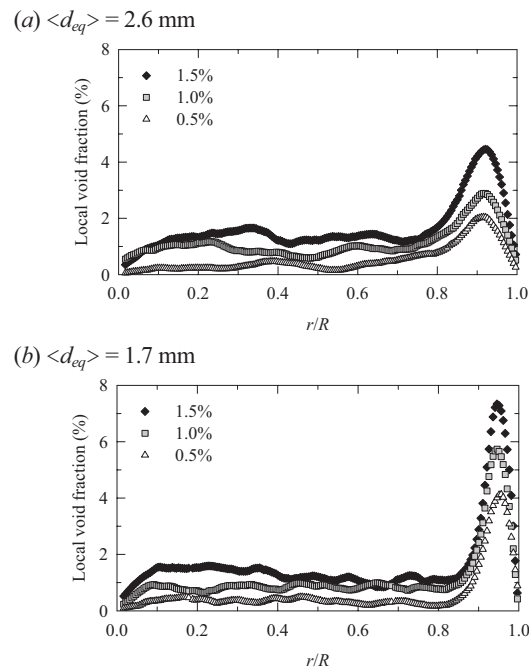


Figure 2 : Profiles of local void fraction of (a) large and (b) small bubbles.

frame rate of 500 Hz smaller than the Kolmogorov time scale of 120 ms, which enable us to resolve the dissipative process of turbulence. Each velocity vector measured by PTV was used to reconstruct grid velocity fields by spatially averaging velocity vectors. The grid size of 200 μ m was smaller than the Kolmogorov length scale of 330 μ m at the centerline, which is reasonably high to resolve the TKE dissipative scale and to obtain the TKE dissipation. The PTV experimental error is estimated to be 1.2% at 95% confidence limits. For SPI, blue LEDs (473 nm) illuminated bubbles from behind. The same type of high speed CMOS camera as PTV was used to capture the projected images of bubbles. The focal plane was set to be identical to the PTV laser sheet plane. Bubbles on the focal plane were detected by recognizing the edge of the bubbles, which have high contrast.

RESULTS AND DISCUSSIONS

Local Void Fraction

The local void fraction, α , which was the ratio of the gaseous to the liquid phase, was calculated by the ratio of the area of bubbles to the area of the imaged section. Figure 2 shows the local void fraction profiles in the presence or large ($\langle d_{eq} \rangle = 2.6$ mm) and small ($\langle d_{eq} \rangle = 1.7$ mm) bubbles. The local void fractions near the pipe wall region are noticeably high due to the shear induced lift force acting on bubbles. For $\langle d_{eq} \rangle = 2.6$ mm, the local void fraction peak appeared at $r/R \approx 0.92$, while it is at $r/R \approx 0.95$ for $\langle d_{eq} \rangle = 1.7$ mm. The shear induced force is depending on the bubble diameter and the non-uniformity trend is greater for the small bubble case.

Mean and RMS Velocities of Liquid Phase

The profiles of streamwise mean velocity of water in the presence of bubbles are shown in figure 3. Since bubbles accelerate the fluid velocity near the wall region, the entire

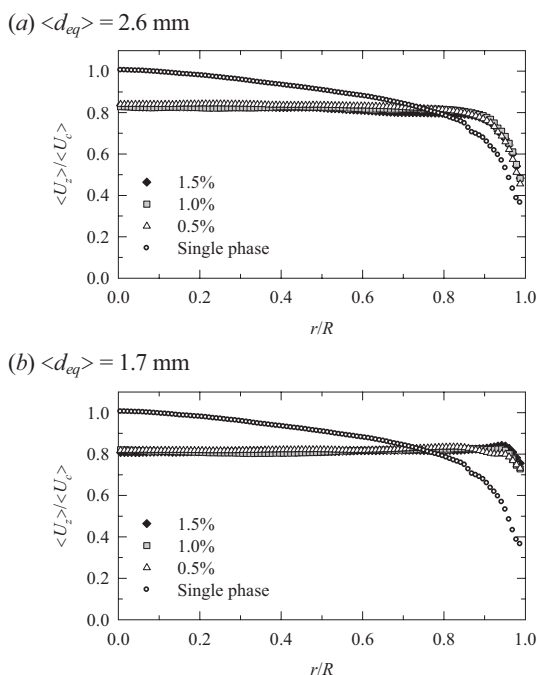


Figure 3 : Profiles of streamwise mean velocity of water in the presence of (a) large and (b) small bubbles.

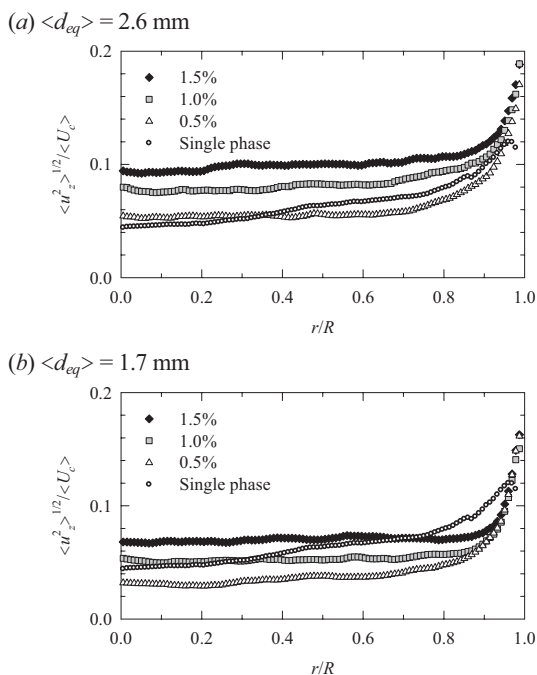


Figure 4 : Profiles of streamwise turbulent intensity of water in the presence of (a) large and (b) small bubbles.

mean velocity becomes flat. This trend is greater for $\langle d_{eq} \rangle = 1.7\text{ mm}$ case and the position where the steep mean velocity gradient appeared was almost the same as the local void fraction peak. This indicates that bubbles block the effect of the shear due to the wall and change the shear-induced turbulence structure. Most bubbles are concentrated near the wall for a dilute ($\alpha = 0.5\%$) bubbly flow to create flattened mean velocity profiles. For higher void fraction, the local void fraction increases more uniformly and they do not affect the

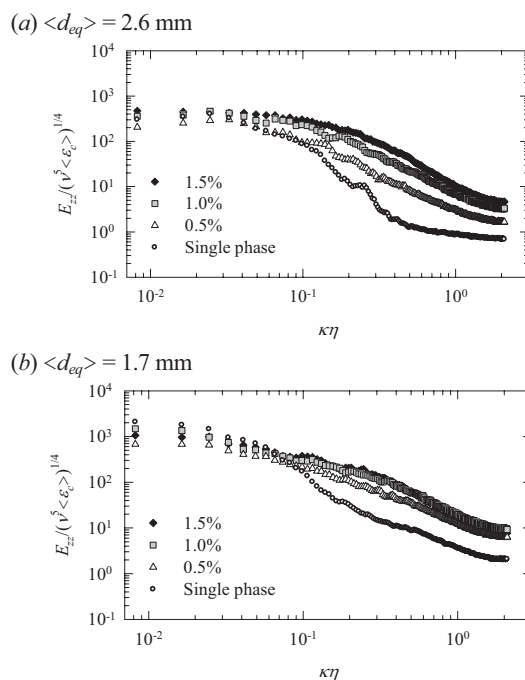


Figure 5 : Profiles of streamwise velocity power spectrum of water in the presence of (a) large and (b) small bubbles at the pipe centerline ($r/R = 0.0$).

mean velocity profile much.

The profiles of streamwise turbulence intensity in the presence of large bubbles are shown in figure 4. The turbulence intensity at $\alpha = 0.5\%$ decreased in the region of $0.4 < r/R < 0.95$ due to the flattened mean velocity profiles by the bubbles, while it increased around the pipe center region due to the presence of bubble wakes ($r/R < 0.4$). At the higher void fraction than 0.5%, the turbulence augmentation at the entire pipe is observed due to the bubble wakes, because the local void fraction increases more uniformly for higher α than 0.5% in the middle of the pipe ($r/R < 0.8$). For the small bubble case, the similar trends are observed. However, the turbulence attenuation trends are greater than those for the larger bubbles due to the greater non-uniformity of the local void fraction.

Turbulence Kinetic Energy Spectra

As described in the previous section, bubbles attenuate large scale turbulence intensity by reducing mean shear flow and to augment large scale turbulence due to bubble wakes. Thus, mechanisms of turbulence modification by bubbles are different at different scales such as Kolmogorov scale, energy containing eddy scale, bubble diameter. The turbulence modification depending on scales by considering the modification in wavenumber space was examined. Turbulence kinetic energy spectra at the pipe centerline in the streamwise direction are shown in figure 5. By assuming the Taylor's hypothesis, the spectra were defined as:

$$E_{ii}(\kappa) = \int_0^{T(U_z)} \left| u_i(t(U_z)) e^{-i\kappa(t(U_z))} \right|^2 d(t(U_z)), \quad (1)$$

where T is the measuring time. Since the Fourier transform of the intermittent liquid-phase due to the gaseous phase is not strictly defined, a linear interpolation for the intermittence of

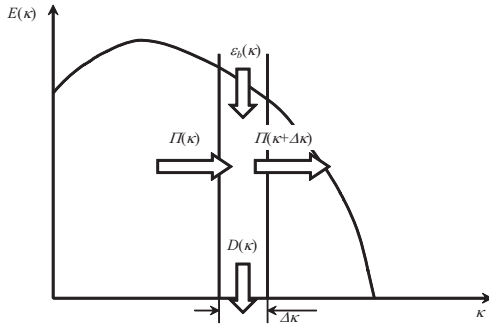


Figure 6 : Concept of energy transport by bubbles in wavenumber space.

the liquid-phase was applied. The vertical axis is normalized by the kinematic viscosity of water, ν , and the energy dissipation rate at the centerline for unladen case, ε_c , where the TKE dissipation was obtained by using a correction method introduced by Tanaka & Eaton (2007) in order to eliminate the measurement noise.

For $\langle d_{eq} \rangle = 2.6$ mm case, the energy spectrum monotonically increased at almost entire scales as the void fraction increased. The augmentation trends are the greatest around $\kappa\eta \approx 10^{-1}$, which is about ten times the bubble diameter. Since the TKE production due to the mean shear is expected to be negligibly small due to the flattened mean flow profiles in the pipe center region, the turbulence augmentation effects are mainly caused by the bubble wakes.

For $\langle d_{eq} \rangle = 1.7$ mm case, the turbulence level at the large scale ($\kappa\eta < 5 \times 10^{-2}$) reduced at $\alpha = 0.5$ due to the flattened mean flow profile. Since the turbulence augmentation at the small scale due to bubble wakes barely increased because of the low local void fraction at the center for $\alpha = 0.5$ case, the total turbulence intensity attenuated as shown in figure 4(b). As the void fraction increases, the TKE increases by the distortion around the bubbles not only at the scale of bubble size but also at the larger scales. This implies that the bubbles induce various size of eddies by clustering.

Scaling Analysis of Turbulence Modification by Bubbles

In the previous sections, we phenomenologically observed that the bubbles modified the large eddies related to the mean flow and small scale eddies due to the wakes. Although the energy spectrum provides much fruitful information, it is not enough to understand the interactions among the large scale flows, small scale turbulence structures and bubbles. In this section, we investigate the modification of the TKE cascade from large to small eddies in order to obtain physical guidance on the modeling for the numerical simulations. We introduce an analytical method to clarify the physical mechanisms of turbulence modification at each scale, or wavenumber. The filtering technique derived from large eddy simulation (LES) is experimentally applied as used in previous studies by Liu *et al.* (1994, 1999) for jet flows to improve LES models by evaluating turbulent kinetic energy flux from large to small eddies. The energy flux is considered as the energy cascade. In the present study, we expand the filtering technique, detailed properties of energy cascade are examined.

First, a general description of LES is recounted before the detailed procedures for the scaling analysis is described. The fluid equations for LES are obtained by filtering the velocity field using a low-pass filtering function, G^Δ , which satisfies the normalization condition. In the current study, we used the sharp cutoff filter, G_S^Δ . The property in one dimension is below.

$$G_S^\Delta(\xi) = \frac{1}{\pi\xi} \sin\left(\frac{\pi\xi}{\Delta}\right), \quad (2)$$

where Δ is the specified filter width. The filtered TKE transport equation for the unresolved or subgrid scale (SGS) can be derived by defining SGS kinetic energy, k_{SGS} , as:

$$\frac{\overline{D}}{Dt} k_{SGS} = \overline{\Pi} - \varepsilon_{SGS} + \frac{\partial T_{SGS}}{\partial x_j} - \varepsilon_{b,SGS}, \quad (3)$$

$$k_{SGS} = \frac{1}{2} (\overline{u_k u_k} - \overline{u_k} \overline{u_k}), \quad (4)$$

where $\overline{(\cdot)}$ and \overline{D}/Dt represent the filtering and the filtered substantial derivative, respectively. T , ε and ε_b denote the energy transport, the energy dissipation, and the energy transfer from bubbles. Each term is defined as:

$$\overline{\Pi} = -\tau_{ij} \overline{S}_{ij}, \quad (5)$$

$$\varepsilon_{SGS} = \nu \left(\overline{\frac{\partial u_k}{\partial x_j} \frac{\partial u_k}{\partial x_j}} - \frac{\partial \overline{u_k}}{\partial x_j} \frac{\partial \overline{u_k}}{\partial x_j} \right). \quad (6)$$

The energy flux, $\overline{\Pi}$, represents the energy exchange from resolved eddies to the SGS eddies. Thus, $\overline{\Pi}$ is the energy source term for SGS kinetic energy equation similar to the TKE production in RANS. The subscript, SGS, represents subgrid scale.

Next, the scaling analysis method we introduce is described as follows based on the filtering techniques. The analysis is conducted in the wavenumber space as shown in figure 6. Considering the TKE energy budget an arbitrary wavenumber, κ , an energy conservation of a tiny control wavenumber domain in between κ and $\kappa + \delta\kappa$ can be written as:

$$\overline{\Pi}(\kappa) + \varepsilon_b(\kappa)\Delta\kappa - D(\kappa)\Delta\kappa = \overline{\Pi}(\kappa + \Delta\kappa), \quad (7)$$

where TKE dissipation spectrum, $D(\kappa)$, and the energy term due to bubbles, $\varepsilon_b(\kappa)$, are described as:

$$D(\kappa) = -\frac{\partial \varepsilon_{SGS}(\kappa)}{\partial \kappa}, \quad (8)$$

$$\varepsilon_b(\kappa) = \frac{\partial \overline{\Pi}(\kappa)}{\partial \kappa} + D(\kappa), \quad (9)$$

Using these equations, we can specify the behaviors of the TKE energy cascade process. This method is expected to investigate various complicated flow fields such as multiphase flow. Also, we emphasize that the current approach can calculate the energy transport by bubbles, which is very complicated term in the TKE equation (Eq. (3)).

An instantaneous energy flux, $\overline{\Pi}$, in the presence of bubbles are shown in figure 7, where the filter width, Δ , was 2.5 mm. The positive regions express the TKE energy from larger to the smaller eddies than the filter width, or TKE forward scatter. The negative ones are TKE energy back scatter. For $\langle d_{eq} \rangle = 2.6$ mm case, bubbles strongly induced both forward and back

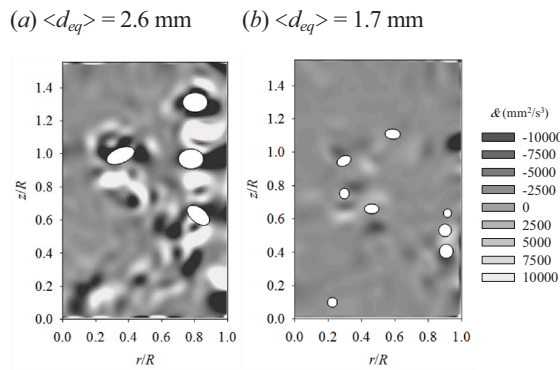


Figure 7 : Contour of energy flux from large to small scales by (a) large and (b) small bubbles. The filter width was set to be $\Delta = 2.5$ mm. The void fraction was 1.5%.

TKE scatters. Since the scattering patterns are characterized in front or behind bubbles, they may possibly be determined by the fluids-bubble relative velocity though further statistical investigation is required. These modified energy flux due to bubbles results in the modification of the TKE spectrum. For $\langle d_{eq} \rangle = 1.7$ mm case, the local modification of the energy flux by bubbles is small. The smaller bubbles do barely disturb local fluids.

The energy flux, Π , as a function of wavenumber are calculated using the measured velocity fields at $0 < r/R < 0.66$ as shown in figure 8. The horizontal axis is normalized by the Kolmogorov length scale, η , at the centerline for single-phase flow. It is observed that the energy flux for single-phase flow monotonically decreased as the wavenumber increases. This indicates that the TKE transported from the large eddies from small scales while it gradually dissipated at each scale. In the presence of $\langle d_{eq} \rangle = 2.6$ mm bubbles, the profiles had peaks around $\kappa\eta \approx 0.07-0.09$. This implies that the energy from bubbles transports to the fluid flows around this scale, resulting in the augmentation of the energy flux. The energy flux increased as the void fraction increased because the energy transport between the liquid-phase and bubbles was promoted. In the presence of $\langle d_{eq} \rangle = 1.7$ mm bubbles, the energy flux attenuated for both $\alpha = 0.5\%$ and 1.0% cases, because of the suppression of the large scale turbulence due to the flattened mean flow. Compared with $\langle d_{eq} \rangle = 2.6$ mm case, the attenuation effect was larger. This is because the local void fraction is smaller and the augmentation due to the bubble wakes is also small for $\langle d_{eq} \rangle = 1.7$ mm. The profiles also had peaks around $\kappa\eta \approx 0.07-0.09$.

The energy due to bubbles, ε_b , as a function of wavenumber, was calculated using the measured velocity fields at $0 < r/R < 0.66$ as shown in figure 9. Strong energy transport from bubbles can be clearly observed for both $\langle d_{eq} \rangle = 2.6$ mm and 1.7 mm cases. The bubble term augmented as the void fraction increased. The peaks appeared at $\kappa\eta \approx 0.05-0.06$ for $\langle d_{eq} \rangle = 2.6$ mm and at $\kappa\eta \approx 0.06-0.066$ for $\langle d_{eq} \rangle = 1.7$ mm. We confirmed that the smaller bubbles induced TKE at smaller scales. By defining the peak wavenumber, κ_b , we attempt to nondimensionalize the peak wavenumber by the bubble diameters. The normalized peak wavenumbers, $1/(\kappa_b \langle d_{eq} \rangle)$, in the present study were:

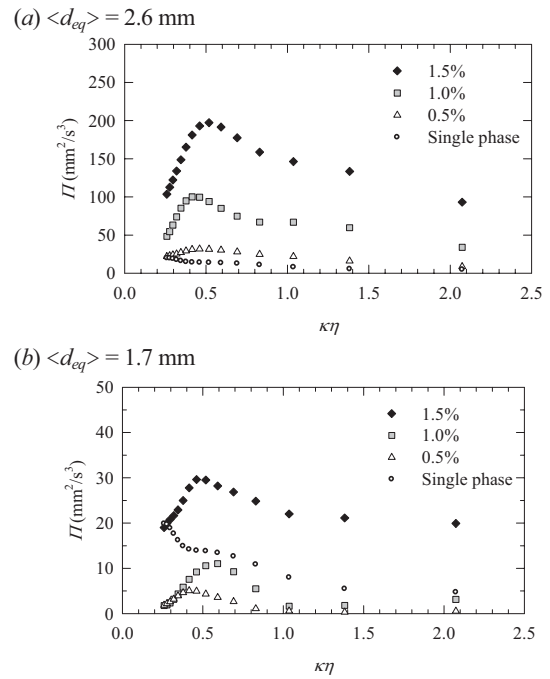


Figure 8 : Profiles of energy flux by (a) large and (b) small bubbles in wavenumber space.

$$2.1 < \frac{1}{\kappa_b \langle d_{eq} \rangle} < 2.6 \quad \text{for } \langle d_{eq} \rangle = 2.6 \text{ mm}, \quad (10)$$

$$2.9 < \frac{1}{\kappa_b \langle d_{eq} \rangle} < 3.2 \quad \text{for } \langle d_{eq} \rangle = 1.7 \text{ mm}, \quad (11)$$

Thus, the TKE transported due to bubbles are at the scale of from two to three times the bubble diameter for similar flow regimes to the present experiment. The interactions between bubbles and the fluids are predominant at this scale. The scale could be applied to determine the filter width in modeling LES.

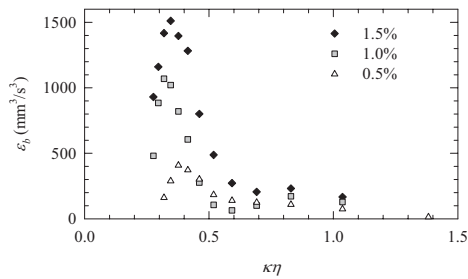
CONCLUSIONS

Turbulence modification in an upward bubbly pipe flow at $Re_{2R} = 9,900$ was investigated using a sub-Kolmogorov PTV/SPI measurement system. Experiments were conducted at two different bubble diameters of 1.7 mm and 2.6 mm and the void fraction up to 1.5 . The findings in the present study are as follows.

The mean flow profiles were flattened in the presence of bubbles because bubbles accumulated near the wall region and accelerated the liquid-phase fluid. The flattened mean flow profiles reduced the shear-induced turbulence intensities in the pipe middle region. The turbulence attenuation trend due to the non-uniformity of the local void fraction was greater for small bubble case ($\langle d_{eq} \rangle = 1.7$ mm). On the other hand, at the higher void fraction than 0.5% , turbulence augmentation at the entire pipe is observed due to the bubble wakes. The trends of turbulence augmentation due to the bubble wakes were larger for large bubbles.

A scaling analysis using the filtered PTV velocity fields was introduced to characterize the length scales that govern the energy transfer between bubbles and turbulence. The local

(a) $\langle d_{eq} \rangle = 2.6$ mm



(b) $\langle d_{eq} \rangle = 1.7$ mm

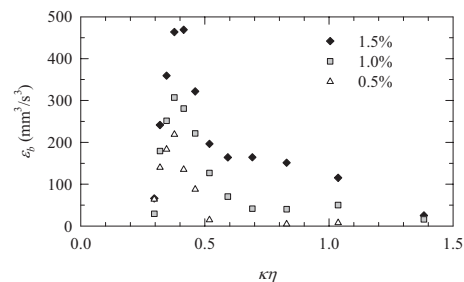


Figure 9 : Profiles of energy transfer due to (a) large and (b) small bubbles in wavenumber space.

energy flux between large and small eddies around bubbles was observed. The energy flux from large to small eddies augmented as the void fraction increased and the profiles had peaks around $\kappa\eta \approx 0.07 - 0.09$, implying that the energy from bubbles transports to the fluid flows around this scale. The energy flux attenuated for both $\alpha = 0.5\%$ and 1.0% cases, for $\langle d_{eq} \rangle = 1.7$ mm because of the suppression of the large scale turbulence due to the flattened mean flow. By calculating the energy due to bubbles, strong energy transport from bubbles was clearly observed in the presence of the bubbles at the scale of from two to three times the bubble diameter. The findings above give guidance on the guidance on the physics and modeling of multiphase flows.

ACKNOWLEDGEMENTS

The authors thank Messrs. M. Koyasu and M. Nakagawa for performing the experiments.

REFERENCES

- Etoh, G.T., Takehara, K., Takano, Y., 2002 "Development of High-speed Video Cameras for Dynamic PIV", *Journal of Visualization*, Vol. 5, pp. 213–224.
- Fujiwara, A., Minato, D., Hishida, K., 2004, "Effect of Bubble Diameter on Modification of Turbulence in an Upward Pipe Flow", *International Journal of Heat and Fluid Flow*, Vol. 25, pp. 481–488.
- Lance, M., Bataille, J., 1991, "Turbulence in the Liquid Phase of a Uniform Bubbly Air-water Flow", *Journal of Fluid Mechanics*, Vol. 222, pp. 95–118.
- Liu, S., Katz, S., Meneveau, C., 1999, "Evolution and Modelling of Subgrid Scales during Rapid Straining of Turbulence", *Journal of Fluid Mechanics*, Vol. 387, pp. 281–320.
- Liu, S., Meneveau, C., Katz S., 1994, "On the Properties of Similarity Subgrid-scale Models as Deduced from Measurements in a Turbulent Jet", *Journal of Fluid Mechanics*, Vol. 275, pp. 83–119.
- Mudde, R.F., Groen, J.S., Van den Akker, H.E.A., 1997, "Liquid Velocity Field in a Bubble Column: Lda Experiments", *Chemical Engineering Science*, Vol. 52, pp. 4217–4224.
- Serizawa, A., Kataoka, I., Michiyoshi, I., 1975, "Turbulence Structure in Air-water Bubbly Flow. II. Local Properties", *International Journal of Multiphase Flow*, Vol. 2, pp. 235–246.
- Tanaka, T., Eaton, J.K., 2007 "A Correction Method for Measuring Turbulence Kinetic Energy Dissipation Rate by PIV", *Experiments in Fluids*, Vol. 42, pp. 893–902.
- Theofanous, T.G., Sullivan, J., 1982, "Turbulence in Two-phase Dispersed Flows", *Journal of Fluid Mechanics*, Vol. 116, pp. 343–362.
- Wang, S.K., Lee, S.J., Jones Jr., O.C., Lahey Jr., R.T., 1987, "3-D Turbulence Structure and Phase Distribution Measurements in Bubbly Two-phase Flows", *International Journal of Multiphase Flow*, Vol. 13, pp. 327–343.